Chemical Engineering Journal Advances 8 (2021) 100138

Contents lists available at ScienceDirect

Chemical Engineering Journal Advances

journal homepage: www.elsevier.com/locate/ceja

Colloidal interactions between model foulants and engineered surfaces: Interplay between roughness and surface energy

Thomas Horseman[a], Zhangxin Wang[b,c], Shihong Lin[a,b,*]

[a] Department of Chemical and Biomolecular Engineering, Vanderbilt University, Nashville, TN, 37235, United States
[b] Department of Civil and Environmental Engineering, Vanderbilt University, Nashville, TN 37235, United States
[c] Guangdong Provincial Key Laboratory of Water Quality Improvement and Ecological Restoration for Watershed, Institute of Environmental and Ecological Engineering, Guangdong University of Technology, Guangzhou 510006, China

ARTICLE INFO

Keywords:
Fouling
Surface roughness
Surface energy
Colloidal interaction
Adhesion

ABSTRACT

Fouling on submerged surfaces is a major limiting factor for membranes, heat exchangers, and marine vessels as it induces mass and heat transfer resistances that increase operating costs and lead to system failures. While the role of surface roughness on fouling has been extensively studied, the specific effect of surface roughness on fouling is debated in literature. In this study, we employed force spectroscopy based on atomic force microscopy with two model colloidal probes to elucidate the role of surface roughness on foulant-surface interactions. Specifically, we quantified the strength and characteristic lengths of the interactions between the colloidal probes and hydrophilic and hydrophobic surfaces with and without surface texture. We found that hydrophilic surfaces are generally less prone to foulant adhesion than hydrophobic surfaces and that increasing roughness of a hydrophilic surface mitigates foulant adhesion. In comparison, we found that increased roughness of a hydrophobic surface increases the attractive foulant-surface interaction, and thus, its fouling propensity. Based on the results from this study, the implications for developing surfaces with fouling resistance are also examined.

1. Introduction

Fouling is a phenomenon that may potentially occur where colloids and organics adsorb to submerged surfaces such as membranes, marine structures, and heat exchangers. Membrane fouling is detrimental as the adsorption of foulants blocks membrane pores, compromising membrane performance and significantly increasing operating costs [1–3]. Heat exchanger fouling is detrimental as the adsorption of foulants adds heat transfer resistance between the two working streams [4,5]. Additionally, fouling on submerged marine surfaces, such as ship vessel hulls, may lead to inferior hydrodynamics, reducing fuel efficiency and increasing overall maintenance costs [6–8]. Because fouling is a major limiting factor for practical applications of membrane technologies, heat exchangers, and marine vessels, the mechanisms and mitigation thereof have been extensively studied [9–18].

Previous studies have investigated the specific behavior of common foulants, including natural organic matters (NOMs), oils, and inorganic colloidal particles [19–24]. Experiments have been performed to elucidate the influence of surface properties, including charge, pore size, and roughness (texture), on the fouling mechanisms in membrane processes [25–31]. However, the effect of surface roughness on fouling in membrane separations is debated. For example, the kinetics of colloidal fouling on reverse osmosis (RO) and nanofiltration (NF) membranes has been shown to positively correlate with membrane surface roughness [32–34]. On the other hand, several studies claim that surface roughness improves the fouling resistance of the membrane by reducing the interaction between foulants and the membrane surface [35–38]. Likewise, there is also debate on the effect of surface roughness and wettability on fouling of vapor-gap membranes (i.e., water does not transport through the membrane in liquid form) such as those used in membrane distillation (MD) and membrane contactors (e.g. for ammonia or methane recovery). For example, humic acid fouling has shown to decrease with increasing hydrophobicity (increased roughness and decreased surface energy) [39–42], while oil fouling can be mitigated altogether by increasing membrane hydrophilicity (increased roughness and surface energy) [43–46]. On the other hand, studies claim that increasing hydrophobicity may slightly increase humic acid fouling [47,48] and oil fouling can be mitigated by increasing membrane hydrophobicity [41].

For marine structures, such as ship vessel hulls, and heat exchangers, particularly those used for seawater cooling and in the food & beverage industry, biofouling is particularly common. Formation of a biofouling layer is predated by the adsorption of soft matter such as bacteria, NOMs, proteins, and oils that serve as precursors for additional foulant attachment [17,49,50]. As such, the fouling behaviors of these species

* Corresponding author at: Department of Civil and Environmental Engineering, Vanderbilt University, Nashville, TN 37235, United States.
E-mail address: shihong.lin@vanderbilt.edu (S. Lin).

https://doi.org/10.1016/j.ceja.2021.100138
Received 19 April 2021; Received in revised form 10 June 2021; Accepted 12 June 2021

and the surface properties that influence the kinetics and strength of their attachment have been extensively studied in these fields [6,51]. However, there is no consensus on the effect of surface roughness and wetting property on the specific fouling behavior of certain organic foulants such as oils, humic substances, or bacteria. For example, increased surface roughness has shown to increase surface area for foulant attachment and increase foulant adhesion for marine vessels or heat exchange surfaces [51–54], while other studies suggest that increased surface roughness may inhibit strong organic foulant attachment depending on the length scale of the surface texture features [55,56]. Likewise, increased surface hydrophobicity (increased roughness and decreased surface energy) has shown to limit organic foulant surface density [57,58], while other studies claim smooth, hydrophobic (low surface energy), surfaces lead to less fouling [59] or that low surface energy surfaces alone (regardless of roughness) mitigate foulant deposition and attachment [60].

To date, no systematic and comprehensive study has been performed to elucidate the combined effect of texture and surface energy on submerged surface fouling. The objective of this study is to systematically investigate the interactions between colloidal probes that mimic representative foulants and model substrates with different morphologies and surface energies, aiming to provide insights for designing fouling-resistant surfaces. To achieve this goal, we constructed smooth and textured silicon dioxide surfaces then grafted them with poly(ethylene glycol) (PEG) and a fluoroalkylsilane (FAS), to obtain smooth and textured hydrophilic and hydrophobic surfaces, respectively. We characterized the surfaces in terms of surface morphology and wetting properties, then performed atomic force microscopy (AFM) force spectroscopy measurements in water with a hydrophilic carboxylate coated polystyrene (C-PS) colloidal probe and a hydrophobic polyethylene (PE) colloidal probe. The maximum adhesion forces and rupture distances between the colloidal probes and surfaces are analyzed to extract insights for developing a framework for fabricating robust fouling resistant surfaces. We note that the study is not intended to focus a specific application, but rather to provide broadly applicable understanding of the dependence of fouling propensity on foulant and surface properties.

2. Experimental section

2.1. Fabrication of surfaces with roughness

Quartz microscope slides (VWR, Radnor, PA) were utilized in this study as the substrate subject to surface modification. To obtain textured surfaces, the slides were rinsed with DI water, followed by sonication, first in ethanol, and then in DI water, each for 10 min. After being dried in air, the slides were immersed in an aqueous dispersion of silica nanoparticles (SiNPs, diameter ~ 200 μm), synthesized using Stöber method [61], with 30 min of sonication. Upon complete evaporation of water in the aqueous solution, slides with surface coated with multiple layers of SiNPs were obtained. The SiNPs-coated slides were then heated at 600 °C for 1 h and purged with pressurized air to remove unassociated impurities. These surfaces were used as the model rough surfaces for further modification.

2.2. Functionalization of surfaces to impart different surface energies

Intrinsic hydrophilicity was imparted to both the smooth and textured surfaces via grafting of poly(ethylene glycol) (PEG) using silane chemistry. Before PEG-grafting, each slide was cleaned by sonication in ethanol and then DI water, each for 10 min, followed by room temperature drying in air, and lastly 5 min of ozone plasma treatment. The cleaned slide was then submerged in a toluene solution with 10 mM HCl and 1 mM 2-[Methoxypoly-(ethyleneoxy)-propyl]trimethoxylsilane (Gelest, Morrisville, PA) for 19 h at room temperature. The modified slides were then rinsed with toluene, ethanol, and DI water, respectively, and dried in an oven at 80 °C for 5 min [62].

Surface hydrophobicity was imparted to both smooth and textured substrates with surface grafting of fluoroalkylsilane (FAS). Similar to grafting of PEG, each slide was sonicated in ethanol and water then treated by ozone plasma. After plasma treatment, the slide and 150 μL of FAS (1H, 1H, 2H, 2H-perfluorodecyltriethoxysilane, Sigma Aldrich, St. Louis, MO) were placed in a Petri dish. The covered Petri dish with the slide and FAS was placed in a vacuum oven at 90 °C for 24 h for vapor deposition. The modified slides were then heated at 80 °C in air for 3 h [63].

2.3. Characterizations of morphology and wetting property

The surface morphology of the smooth and textured model surfaces was observed using both scanning electron microscopy (5 kV, HE-SE2 secondary electron detector, SEM, Merlin, Zeiss, Thornwood, NY), and AFM-based force spectroscopy (ScanAsyst mode, Dimension Icon, Bruker, Billerica, MA). The static liquid contact angles (CAs) of the surfaces were measured with water in air and with mineral oil underwater. All CAs were measured with an optical tensiometer (TL100, Attension, Finland). The in-air CA measurements were performed using sessile drop method, while the underwater oil CA measurements were conducted following captive bubble method with the air bubble replaced by a mineral oil droplet. For each sample, the CAs were measured at five different locations on the surface and averaged with standard deviation reported.

2.4. Colloidal probe force spectroscopy

Force spectroscopy was used to measure the interfacial forces between functionalized colloidal probes (Novascan, Ames, IA) and model surfaces using an AFM (Fig. 1). Two different types of colloidal probes were used, including polyethylene (PE) colloidal probe and polystyrene colloidal probe functionalized with carboxyl groups (C-PS). The PE probe is made of a soft and hydrophobic PE colloidal particle that mimics the behavior of deformable hydrophobic colloidal foulants (e.g. oil droplets and proteins), while the C-PS probe has been used to study the fouling by organic matter that is typically rich in carboxyl groups (e.g. humic acid and algae) [31,64–67]. The diameters for the PE probe and C-PS probe were 5 μm and 4.5 μm, respectively. Force measurements were conducted in 10 mM aqueous solution of NaCl following previous studies [33,68–70]. Other solution chemistries could be used, which would mostly affect the electrical double layer (EDL) interaction. The effects of electrolyte type and concentrations on particle-surface interaction has been extensively studied and well understood [71–73], and thus would not be the focus of this investigation. The trigger force, ramp size, and ramp rate were 5 nN, 2.5 μm, and 1 Hz, respectively. The raw force data was collected by the AFM during the extension (approaching) and retraction regimes of the experiment. For each sample, force spectroscopy was conducted at 300 different positions within a 25 μm^2 area near the center of the surface to obtain interaction force curves that were analyzed using NanoScope Analysis 1.5.

3. Results and discussion

3.1. Morphologies of the surfaces

The morphology of smooth and textured surfaces are drastically different (Fig. 2A & 2B, respectively). Specifically, the presence of SiNPs renders the modified surface significantly rougher than the pristine surface without SiNPs. The deposited SiNPs multi-layer coalesced upon sintering at 600 °C and formed a continuous surface with texture (Fig. 2B). Such a sintering effect also immobilizes the SiNPs so that they do not detach from the surface or move laterally as the colloidal probe interacts with the surface in the force spectroscopy experiments.

The surface morphology of the smooth and textured surfaces was also measured via AFM (Fig. 2C and D, respectively). Similar to the SEM images, the AFM images show that the surface deposited with

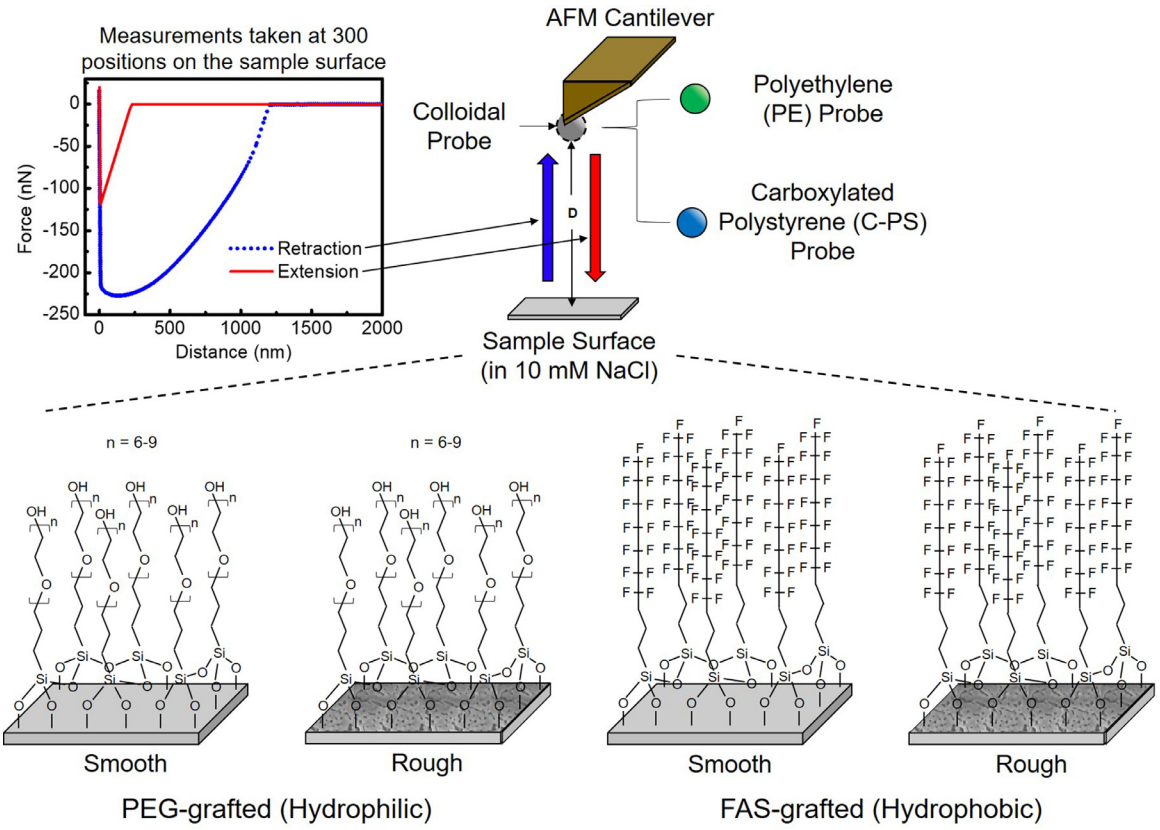

Fig. 1. Schematic diagram showing AFM-based colloidal probe force spectroscopy, featuring representative extension curve (red) and retraction curve (blue). Two colloidal probes were used: a polyethylene (PE) probe that mimics a soft hydrophobic colloidal foulant such as an oil droplet and a carboxylated polystyrene (C-PS) probe with the carboxyl groups representing moieties commonly found in natural organic matter. Model surfaces consisted of hydrophilic poly(ethylene glycol) (PEG) grafted surfaces and hydrophobic fluoroalkylsilane (FAS) grafted surfaces, each with a smooth version and rough version textured with silica nanoparticles. (For interpretation of the references to color in this figure legend, the reader is referred to the web version of this article.) .

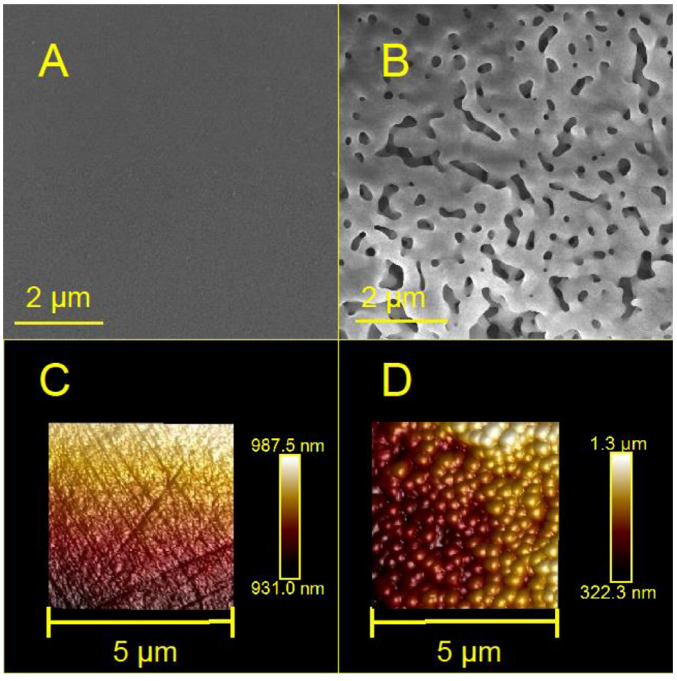

Fig. 2. SEM images of the surfaces of (A) the smooth, pristine, microscope slide and (B) the rough, SiNPs surface multi-layer, slide. The corresponding AFM images of the surfaces (C) the smooth, pristine, slide and (D) the rough SiNPs surface coated slide.

SiNPs (Fig. 2D) is much rougher than the bare, smooth surface (Fig. 2C). Specifically, the measured average roughness (R_a) and root mean square roughness (R_q) of the rough surface are 62.2 and 79.7 nm, respectively, nearly, two orders of magnitude larger than those of the smooth surface (R_a = 0.8 nm, R_q= 1.0 nm).

3.2. *Wetting properties of the smooth and rough surfaces*

The PEG-grafted smooth surface has an in-air water CA of 38.0 ± 0.3° (Fig. 3). In comparison, the in-air water CA of the PEG-grafted rough surface was not detectable, suggesting the surface was rendered superhydrophilic. The CA reduction of a PEG-grafted surface by increasing surface roughness can be explained via Wenzel's theory [74]: if the roughness ratio of the surface, defined as the ratio of actual surface area over the projected surface area, is *r*, the apparent CA of a rough surface, θ_A, deviates from the intrinsic CA of a smooth surface with the same surface tension, θ_0, following the equation below [75]:

$$\cos\theta_A = r\cos\theta_0 \quad (1)$$

The Wenzel's theory suggests that increasing surface roughness will amplify the hydrophilicity of an intrinsically hydrophilic surface and render the surface superhydrophilic.

For the FAS-grafted surfaces, the in-air water CAs of the smooth and rough surfaces were 109.2 ± 0.2° and 134.5 ± 0.8° (Fig. 3), respectively. The introduction of roughness to the surface enhanced the apparent CA of the hydrophobic surface. However, due to the roughness imparted on the rough FAS-grafted surface, the water droplet exists in a Cassie-Baxter state, where the droplet is supported by not only the FAS-grafted surface, but also air pockets within the surface roughness features [76,77]. In a

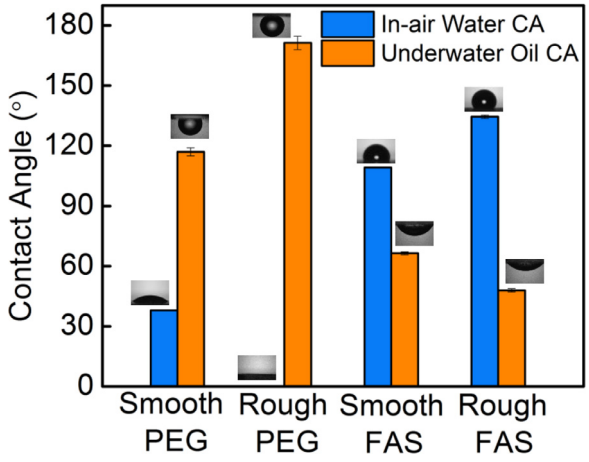

Fig. 3. (Blue) In-air water contact angles of the smooth PEG grafted surface, the rough PEG grafted surface, the smooth FAS deposited surface, and the rough FAS deposited surface. In-air water contact angle images displayed above each respective contact angle value. (Orange) Underwater oil contact angles of the smooth PEG grafted surface, the rough PEG grafted surface, the smooth FAS deposited surface, and the rough FAS deposited surface. Underwater oil contact angle images displayed above each respective contact angle value. (For interpretation of the references to color in this figure legend, the reader is referred to the web version of this article.)

Cassie-Baxter state, the apparent CA, θ_A, relates to the intrinsic CA, θ_0, by the following equation:

$$\cos\theta_A = f\left(\cos\theta_0 + 1\right) - 1 \quad (2)$$

where f is the areal fraction of water-solid contact and thus $(1 - f)$ is the areal fraction of water-air contact. If we assume the roughness on the FAS-grafted silica surface without SiNPs deposition to be negligible, then θ_0 is 109.2 ± 0.2° and f is calculated to be ~0.54.

The FAS-grafted rough surface, with a CA of 134.5 ± 0.8°, is not qualified as a superhydrophobic surface which typically requires an apparent CA higher than 150° In previous studies using surfaces modified with fluorinated SiNPs, superhydrophobicity can be readily achieved [78–84]. Here, sintering SiNPs changed the morphology of deposited SiNPs layer, smoothing the interconnections between SiNPs, and consequently reducing f and reducing the mean curvature of the "surface protrusions". We choose to use such a sintered surface for adhesion force measurement even though it is not superhydrophobic, as we want to prevent, to the greatest extent possible, the potential lateral movement or detachment of SiNPs during the adhesion force measurements. The key feature of the rough surface we want to achieve for comparison with a smooth surface is not a super-high apparent CA, but rather the presence of air pockets that lead to Cassie-Baxter contact between the textured hydrophobic surface and a hydrophobic colloidal probe.

The underwater CAs measured with mineral oil are also presented in Fig. 3. The PEG-grafted smooth surface, which is in-air hydrophilic, is underwater oleophobic with an underwater oil CA of 117.0 ± 2.0° The PEG-grafted rough surface, which is in-air superhydrophilic, is underwater superoleophobic with an ultrahigh underwater oil CA of 171.3 ± 3.3° The oleophobicity (or superoleophobicity) of the PEG-grafted surface is attributable to the hydration force [72,85,86]: for an oil droplet to spread over the PEG-grafted surfaces, the hydrophilic (or superhydrophilic) surfaces have to first be dehydrated. The dehydration of a highly hydrophilic surface submerged in water is thermodynamically unfavorable. In comparison, the FAS-grafted smooth and rough surfaces are both underwater oleophilic due to the attractive hydrophobic-hydrophobic interaction between the oil droplet and the FAS-grafted surface [87–90]. The surface roughness enhanced the underwater oleophilicity of the FAS-grafted surface, reducing the underwater oil CA from 66.4 ± 0.7° to 47.9 ± 0.8° Assuming the system to be in a Cassie-Baxter state (which is consistent with previous experimental observation [1]), f is calculated to be 0.55, very close to the f value estimated using in-air water CA.

3.3. Colloidal probe force spectroscopy

3.3.1. Force curves characteristic of different interactions

The force measured via AFM-based colloidal probe force spectroscopy regards the interaction between the colloidal probe and substrate surface at different separation distances (**Fig. 4**). Each force curve comprises two regimes, with the colloidal probe approaching the substrate surface in the first regime (extension) and pulling off from the substrate surface in the second regime (retraction). In the absence of interaction between the colloidal probe and the substrate surface, the baseline interaction force was zero in the initial stage of the extension regime and the final stage of the retraction regime. As the probe approached the surface in the extension regime and pulled off from the surface in the retraction regime, force curves of different shapes were observed with different combinations of colloidal probes and substrate surfaces. The representative extension and retraction curves are presented in Fig. 4. Due to the large number of scenarios Fig. 4 covers, we will first focus on comparing the extension force curves (in red) for different scenarios, then move on to compare the retraction force curves (in blue).

3.3.2. The extension curves

PE probe with PEG-grafted surfaces For the PE colloidal probe, which represents a soft, hydrophobic, colloidal particle such as an oil droplet or protein, a small and relatively short-ranged attraction was observed for interaction with the smooth and rough PEG-grafted surfaces (red curves in Fig. 4A and B). This relatively short-ranged attractive interaction results from a stronger attractive van der Waals (vdW) interaction as compared to the repulsive electrical double layer (EDL) interaction throughout the range of separation [91–93]. The magnitude of the attractive interaction, however, was very small. In both cases, the maximum net attractive force was lower than 1 nN. In addition, repulsive force, if there was any, was also negligibly small in either case.

PE probe with FAS-grafted surfaces The interactions between the PE colloidal probe and the FAS-grafted surfaces (red curves in Fig. 4C and D) in the extension regime strongly depend on the surface roughness. With a smooth FAS-grafted surface, the interaction was qualitatively similar to that with a smooth PEG-grafted surface for being attractive and relatively short-ranged (red curve in Fig. 4C). However, the magnitude of the interaction was an order of magnitude higher, possibly due to hydrophobic interaction [89,94]. The interaction of the PE colloidal probe with a rough FAS-grafted surface was drastically different from those with PEG-grafted surfaces.

With an FAS-grafted textured surface, the attractive interaction was long-ranged and orders of magnitude stronger (red curve in Fig. 4D). One possible explanation is that sub-micron scale air films might be present on the rough hydrophobic surface that sustains a Cassie-Baxter state [95–97]. The contact between the approaching colloidal probe and such air films, which occurred at a significantly longer range than that for vdW interaction, resulted in capillary force that was significantly stronger than the what would have been predicted by the classic Derjaguin-Landau-Verwey-Overbeek theory considering the van der Waals (vdW) and electrical double layer (EDL) interactions [67,89,98–100].

C-PS probe with PEG-grafted surfaces The carboxylated polystyrene (C-PS) colloidal probe behaved slightly differently from the PE colloidal probe in the extension regime when interacting with the PEG-grafted surfaces (red curves in Fig. 4E and F). A discernable force barrier was detected when the C-PS probe approached the smooth PEG-grafted surface, likely due to the stronger repulsive EDL interaction and hydration force (red curve in Fig. 4E). Although the PE colloidal probe can possibly acquire surface charge via ion adsorption [101–103], its surface

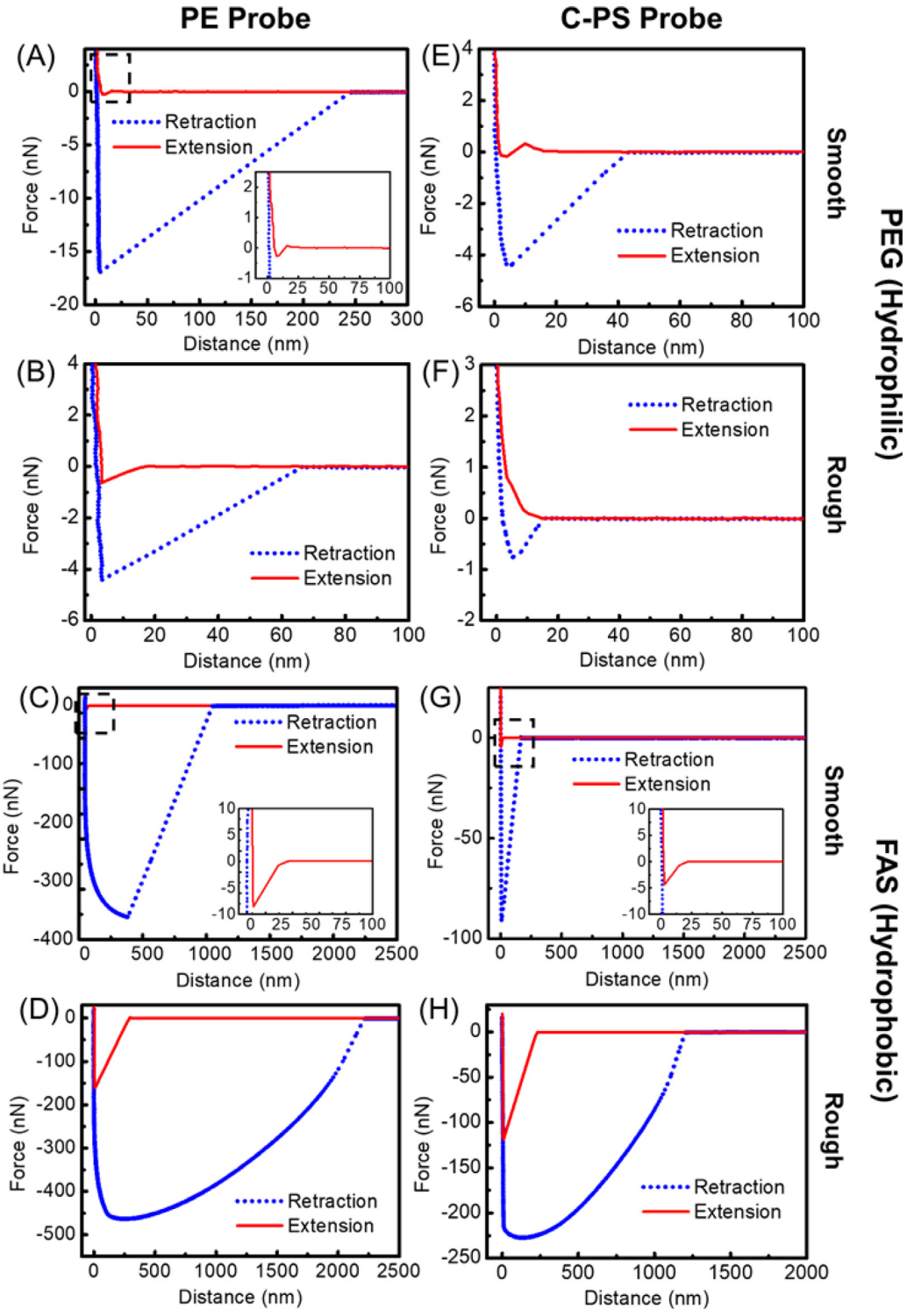

Fig. 4. Representative AFM force curves of polyethylene (PE) colloidal probe interacting with (A) a smooth hydrophilic PEG grafted surface, (B) a rough hydrophilic PEG grafted surface, (C) the smooth hydrophobic FAS grafted surface, and (D) a rough hydrophobic FAS grafted surface, respectively. Representative AFM force curves of carboxylate coated polystyrene (C-PS) colloidal probe interacting with (E) a smooth hydrophilic PEG grafted surface, (F) a rough hydrophilic PEG grafted surface, (G) a smooth hydrophobic FAS grafted surface, and (H) a rough hydrophobic FAS grafted surface, respectively. We note the substantial difference in the y-axis range between panels (A, B, E, F) and panels (C, D, G, H). (For interpretation of the references to color in this figure, the reader is referred to the web version of this article.)

charge/potential should be substantially lower than that the C-PS probe that is functionalized with abundant surface carboxylate groups [104]. Thus, the PE probe is hydrophobic and weakly charged, whereas the C-PS probe is hydrophilic and highly negatively charged. As a result, stronger repulsion from EDL interaction and hydration force leads to a discernable force barrier in the interaction between C-PS probe and the smooth PEG-grafted surface, which was hardly observed with the PE probe. When it comes to the rough PEG-grafted surface, the interaction was entirely repulsive and no net attractive force was observed, which can possibly be explained by the stronger hydration force due to the enhanced contact area for interaction with a rough surface (red curve in Fig. 4F).

C-PS probe with FAS-grafted surfaces The interactions of the C-PS probe with the smooth and rough FAS-grafted surfaces (red curves **in** Fig. 4G and H) were similar to that with the PE probe (red curves in Fig. 4C and D). Compared to the interaction between PE probe and the smooth FAS grafted surface (red curve in Fig. 4C), the attractive force between the C-PS probe and the smooth FAS-grafted surface (red curve in Fig. 4G) was slightly weaker and shorter-ranged without the hydrophobic-hydrophobic interaction. Furthermore, with the interaction between the C-PS probe and the smooth FAS-grafted surface (red curve in Fig. 4G), a more appreciable attractive force was observed compared to that observed with the smooth PEG-grafted surface (red curve in Fig. 4E), possibly due to the lack of hydration layer on the FAS-grafted surface. When it comes to interacting with the rough FAS-grafted surface (red curve in Fig. 4H), the C-PS probe experienced a very long-ranged and strong attractive interaction (>100 nN), similar to that observed with the PE probe (red curve in Fig. 4D). Similar to the interaction between PE probe and the rough, FAS-grafted surface, the submicron sized air film formed on a rough hydrophobic surface is responsible for this long-ranged and strong attractive interaction of capillary nature.

Overall, during the extension regime in AFM-force spectroscopy experiments, the interactions measured between colloidal probes and substrate surfaces were dramatically different depending on the physico-chemical properties of the probe and the substrate, and the substrate morphology. In general, the differences result from the interplay between several possible interactions, including: EDL repulsion, vdW attraction, short-ranged repulsion from hydration force, the relatively short-ranged attractive hydrophobic interaction, and the very long-ranged attractive interaction due to capillarity. While the specific interactions at hand depend on the physico-chemical properties of the probe and substrate, roughness was generally found to enhance the interaction force, whether attractive or repulsive, compared to that of a smooth surface of the same surface chemistry. We note that the experimental results from the extension force curves correspond well to the previous fouling experimental studies. For the hydrophobic surfaces, the increase of roughness would increase the attraction force between foulants and the surface, and thereby facilitate fouling [32–35,105,106]. However, the roughness increased on hydrophilic surfaces would increase the repulsive force between foulants and the surface, and consequently improve the fouling resistance [36–38,43–46,54,105,107,108].

3.3.3. The retraction curves

PE-probe with PEG-grafted surfaces For the interaction between PE colloidal probe and the smooth and rough PEG-grafted surfaces, a small (<20 nN) and relatively short-ranged attraction was observed during the retraction regime (blue curves in Fig. 4A and B). The short-ranged attractive forces attributed to vdW interaction were interestingly stronger and longer-ranged on the smooth PEG-grafted surface (blue curve in Fig. 4A) than they were with the rough PEG-grafted surface (blue curve in Fig. 4B). Such a difference is attributable to the differences in contact area between the soft PE colloidal probe and the two PEG-grafted surfaces with different morphologies. More probe-surface contact area is expected with the smooth PEG-grafted surface compared to the rough PEG-grafted surface at the beginning of the retraction regime, as the size of the probe (5 μm) is substantially larger than the “pores” on the SiNPs-constructed rough surface. Consequently, the larger area of contact between the PE probe and the smooth, PEG-grafted surface led to stronger and longer-ranged attraction in the retraction regime.

PE-probe with FAS-grafted surfaces As in the extension regime, the interactions of the PE colloidal probe with the FAS-grafted surfaces in the retraction regime strongly depend on the surface morphology (Fig. 4C and D). However, the interaction was closer in magnitude than it was in the extension regime. In general, the interaction between the PE colloidal probe and the smooth FAS-grafted surface was less attractive and shorter-ranged than that with the rough FAS-grafted surface, which further confirms the presence of long-range capillary interaction caused by the presence of the air film on the rough hydrophobic surface that sustains a Cassie-Baxter state [95–97]. Furthermore, we note the interactions between PE colloidal probe and FAS-grafted surfaces were two orders of magnitude stronger and around one order of magnitude longer-ranged than that with the PEG-grafted surfaces, due to the relatively long-ranged hydrophobic-hydrophobic interaction with the smooth FAS-grafted surface and the very long-ranged capillary interaction with the rough FAS-grafted surface.

C-PS probe with PEG-grafted surfaces The interaction between the carboxylated polystyrene (C-PS) colloidal probe was similar to that of the PE colloidal probe in the retraction regime, when interacting with the PEG-grafted surfaces (blue curves in Fig. 4E and 4F). For example, the interactions were small (<5 nN) and relatively short-ranged regardless of the surface morphology, but were comparatively stronger and longer-ranged with the smooth PEG-grafted surface (blue curve in Fig. 4E) than with the rough PEG-grafted surface (blue curve in Fig. 4F). The stronger interaction with a smooth surface is again attributable to the larger contact area between the C-PS colloidal probe and the smooth, PEG-grafted surfaces.

C-PS probe with FAS-grafted surfaces The interactions of the C-PS probe with the smooth and rough FAS-grafted surfaces in the retraction regime (blue curves in Fig. 4G and H) qualitatively resemble that of the PE probe (blue curves in Fig. 4C and D). However, the attractive interaction between the C-PS probe and the smooth FAS-grafted surface was slightly weaker and shorter ranged than the interaction between PE probe and smooth FAS-grafted surface without the presence of the hydrophobic-hydrophobic interaction. Furthermore, a more appreciable attractive force was observed with the interaction between the C-PS probe and the smooth FAS-grafted surface (blue curve in Fig. 4G) compared to that observed with the smooth PEG-grafted surface (blue curve in Fig. 4E) due to the lack of hydration layer on the FAS-grafted surface. As for the interaction with the rough FAS-grafted surface (blue curve in Fig. 4H), the C-PS probe experienced a very long-ranged and strong attractive interaction (>200 nN), similar to that observed with the PE probe (blue curve in Fig. 4H). Again, we attribute this strong and long-ranged interaction of capillary nature to the presence of submicron sized air film on the rough hydrophobic surface.

In general, the interactions measured between the colloidal probes and substrate surfaces in the retraction regime were more attractive and longer-ranged in nature than those measured during the extension regime. However, the magnitudes of the attractive forces and the range of interactions differed among the specific colloidal probe-substrate surface pairings. On the hydrophilic PEG-grafted surfaces, roughness was generally found to decrease the attractive interaction compared to that of the smooth surface, likely due to a decrease in probe-surface contact area. While on the hydrophobic FAS-grafted surfaces, roughness was generally found to increase the attractive interaction compared to that of the smooth surface, likely due to capillary forces because of the presence of an air film at the rough hydrophobic surface. These capillary forces result in a nonlinear retraction force curve which is likely due to a capillary bridge that forms between the surface and probe, changing in geometry and changing the degree of dewetting as it moves away from the surface [65,89]. The interactions measured in the retraction regime suggest that removal of foulants would be easiest for textured hydrophilic surfaces.

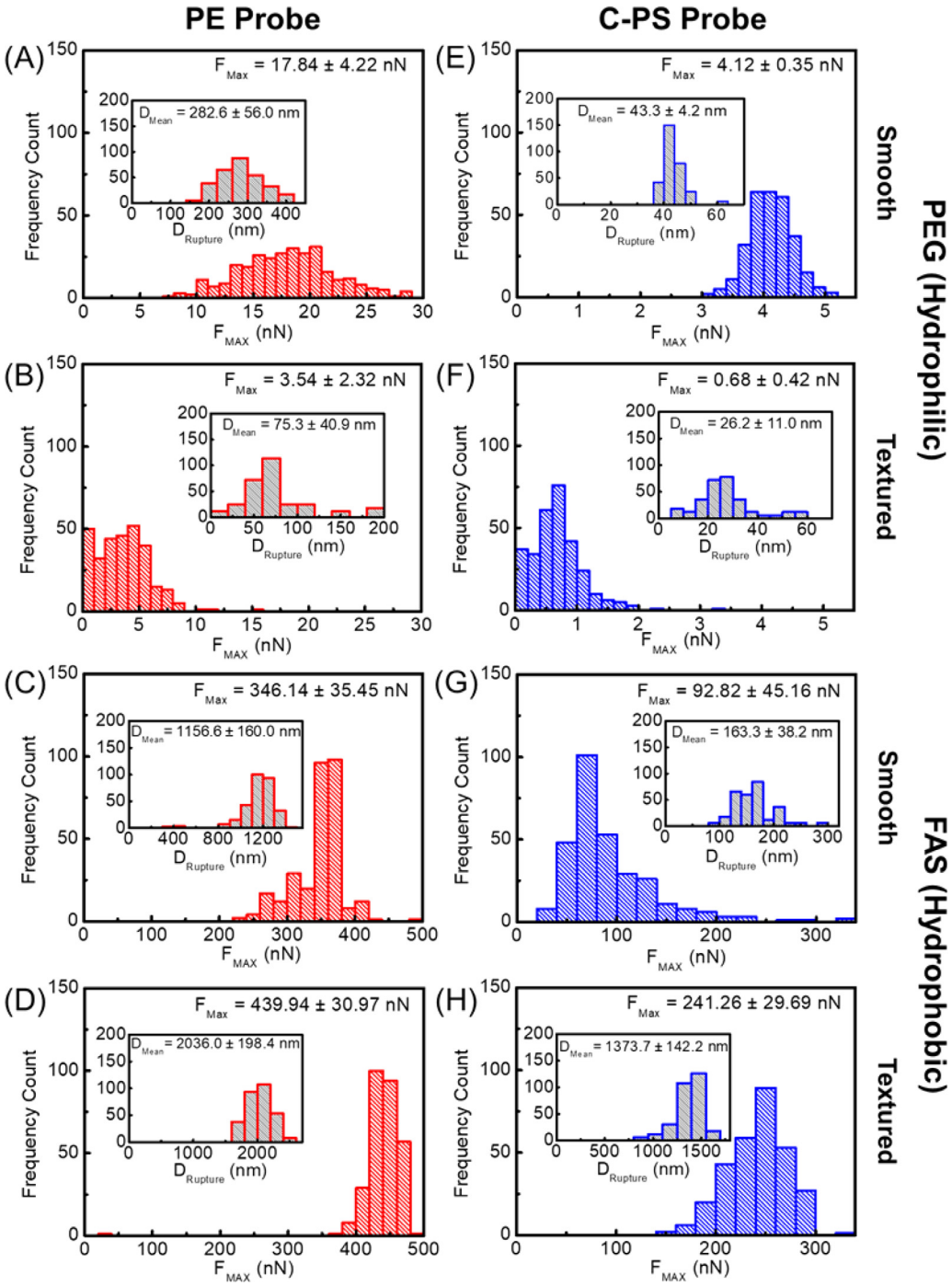

Fig. 5. Distributions of max adhesion force (F_{Max}) and rupture distances ($D_{Rupture}$, insets) measured at 300 different positions on the sample surfaces. Adhesion statistics of polyethylene (PE) colloidal probe interacting with (A) the smooth hydrophilic surface, (B) the rough hydrophilic surface, (C) the smooth hydrophobic surface, and (D) the rough hydrophobic surface, respectively. Adhesion statistics of carboxylated polystyrene (C-PS) colloidal probe interacting with (E) the smooth hydrophilic surface, (F) the rough hydrophilic surface, (G) the smooth hydrophobic surface, and (H) the rough hydrophobic surface, respectively.

3.4. Adhesions between the colloids and the surfaces

The discussion in Section 3.3 is based primarily on representative force curves, each chosen from hundreds of repetitive force measurements at different locations on the model surface. The retraction regime of each force curve yields two key characteristic parameters, the maximum adhesion force, and the rupture distance. The maximum adhesion force is the maximum force measured while retracting the colloidal probe from the substrate surface. This adhesion force is directly related to the net adhesion energy (W_{PS}) between the probe (P) and substrate (S). In the three-phase system consisting of water (L), substrate, and probe, the balance of interfacial energies (γ_{ij}) and contact-area between the probe and substrate (A_{PS}) tends to an energy minimum according to:

$$W_{PS} = A_{PS}\left(\gamma_{SL} + \gamma_{PL} - \gamma_{PS}\right) \tag{3}$$

Rupture distance is the maximum distance where the interaction between the colloidal probe and the substrate surface is no longer present

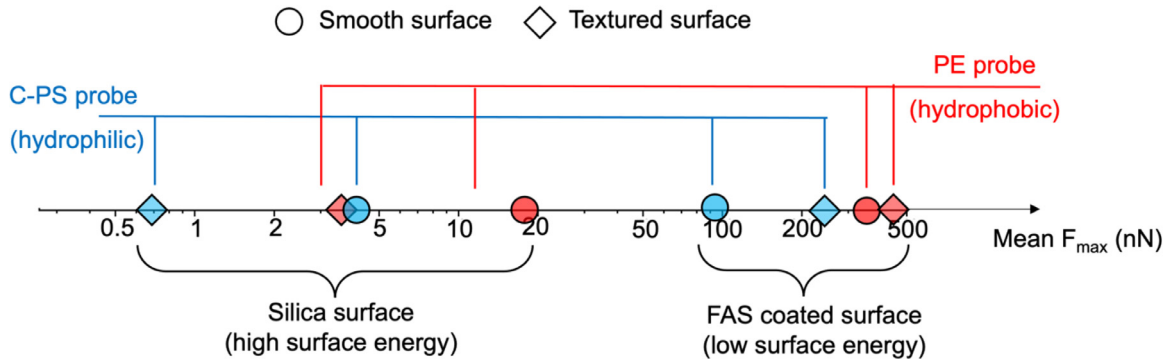

Fig. 6. Comparison between the mean values of maximum adhesion force for different interactions based on data presented in Fig. 5. The axis is in log scale.

Table 1
Adhesion force statistics of the polyethylene (PE) and carboxylate coated polystyrene (C-PS) colloidal probes interacting with the smooth and rough hydrophilic PEG-grafted surfaces and smooth and rough hydrophobic FAS-grafted surfaces.

Probe	Surface Type		Maximum Adhesive Force (nN)	Rupture Distance (nm)
PE	PEG (Hydrophilic)	Smooth	18 ± 4	283 ± 56
		Rough	3 ± 2	75 ± 41
C-PS		Smooth	4.1 ± 0.3	43 ± 4
		Rough	0.7 ± 0.4	26 ± 11
PE	FAS (Hydrophobic)	Smooth	346 ± 35	1157 ± 160
		Rough	440 ± 31	2036 ± 198
C-PS		Smooth	93 ± 45	163 ± 38
		Rough	241 ± 30	1374 ± 142

[109,110]. Strong attractive interactions between the colloidal probes and the substrate surfaces generate larger maximum adhesion forces and larger rupture distances, and vice versa. For each probe-substrate surface pairing, the force curves were measured at 300 locations on the surface, and the distributions of maximum adhesion force and rupture distance were calculated for each pairing (Fig. 5). The mean maximum adhesion forces and mean rupture distances are summarized in Table 1.

For the interactions between colloidal probes and hydrophilic surfaces (Fig. 5A, B, E, and F), the adhesion force is substantially weaker, and the rupture distance is significantly shorter as compared to the interaction with hydrophobic surfaces (Fig. 5C, 5, G, and H). With the same colloidal probe, the maximum adhesion forces and rupture distances measured with the rough hydrophilic surfaces (Fig. 5B and F) are considerably less than those measured with the smooth hydrophilic surfaces (Fig. 5A and E). The hydrophilic surfaces favor contact with water (i.e. surface hydration, $\gamma_{PL} < \gamma_{PS}$ and $\gamma_{SL} < \gamma_{PS}$), so retracting the colloidal probe from the surface and replacing the area A_{PS} with the substrate-water interface, minimizes the net interfacial energy of the three-phase system [72]. According to Eq. (3), γ_{SL}, γ_{PL}, and γ_{PS} are identical for the rough and smooth hydrophilic surfaces in contact with the same colloidal probe. Because the interfacial area, A_{PS}, between the probe and rough hydrophilic surface is less than that with the smooth hydrophilic surface, there is less net adhesive energy, and thus lower max adhesion force that must be overcome to remove the probe from the surface. Likewise, with the same morphology of the hydrophilic surfaces, the maximum adhesion forces measured with the C-PS colloidal probe is smaller than that measured with the PE colloidal probe. This is likely caused by two reasons. Firstly, the PE probe is slightly larger (5 μm diameter) and softer (Young's Modulus ~ 500 MPa) than the C-PS probe (4.5 μm diameter and Young's Modulus ~ 3000 MPa), meaning the interfacial area between the PE probe and substrate (A_{PS} in Eq. (3)) is always greater than that of the C-PS probe for the same surface, resulting in lower maximum adhesive force [72]. Secondly, is the higher degree of hydration of the C-PS probe as compared with the PE probe ($\gamma_{PL,\,C-PS} < \gamma_{PL,\,PE}$), caused by the negatively charged carboxyl groups on the C-PS probe that form hydrogen bonds with water. The hydration of the C-PS probe renders its contact with the hydrophilic substrate energetically unfavorable as it increases the net interfacial energy, and its detachment from the hydrophilic substrate energetically highly favorable.

In general, strong adhesive forces and large rupture distances were observed with rough hydrophobic (FAS-coated) surface regardless of type of colloidal probe (Fig. 5D and H). These strong and long-ranged interactions are attributable to the capillary interaction between the particles and the air-film anchored to the textured hydrophobic surface in the Cassie-Baxter state [89,94,98–100,111]. In particular, the interaction was the strongest between the textured hydrophobic surface and the hydrophobic PE probe (Fig. 5D). However, surface texture is not a pre-requisite for strong and long-ranged attractive interaction which has also been observed between the hydrophobic PE probe and the smooth hydrophobic surface due to the hydrophobic-hydrophobic interaction (Fig. 5C). Specifically, the retraction of the PE colloidal probe from the hydrophobic surface would increase the interfacial area between water and the hydrophobic surfaces and reduce the overall interfacial entropy of the system, rendering a thermodynamically unfavorable state [72]. Such an effect is considerably smaller for interaction between a smooth hydrophobic surface and a C-PS probe that is less hydrophobic than the PE probe (Fig. 5G). The comparison of the average maximum adhesion forces between these different scenario is also summarized in **Fig. 6**.

4. Conclusions

Using AFM force spectroscopy, we elucidate the role of surface texture and surface energy on the interaction between model foulants and surfaces with different morphology and surface energy. We found that: (1) submerged hydrophilic surfaces are generally less prone to fouling than is a submerged hydrophobic surface, which is relatively well known; (2) compared to a smooth hydrophobic surface, a rough hydrophobic surface increases not only the strength but also the characteristic length of the attractive interaction; and (3) compared to a smooth hydrophilic surface, a rough hydrophilic surface reduces not only the strength but also the characteristic length of the attractive interaction. In other words, the surface roughness/texture amplifies the intrinsic interaction between the foulants and a substrate surface, which is similar to how it amplifies the surface wetting properties.

The implications gleaned from this study provide significant insight for fabrication of anti-fouling surfaces used membrane separations, heat exchangers, and marine structures. In general, mitigation of organic fouling, should it be oil or natural organic matter, prefers superhydrophilic surfaces characterized by high surface energy and large roughness. If hydrophobic materials must be used for specific processes, the presence of surface roughness (texture) would result in strong adhe-

sion of hydrophobic foulants due to capillarity, which is unfavorable for mitigating organic fouling. We note that such suggestions apply specifically to organic fouling and that the mitigation of mineral scaling may follow completely different rules.

Declaration of Competing Interest

The authors declare no completing interest.

Acknowledgments

The authors acknowledge the support from American Chemical Society Petroleum Research Foundation via award ACS-PRF 57353 DNI and from National Science Foundation via award 1705048.

References

[1] Z. Wang, S. Lin, Membrane fouling and wetting in membrane distillation and their mitigation by novel membranes with special wettability, Water Res. 112 (2017) 38–47, doi:10.1016/j.watres.2017.01.022.
[2] A.L. Lim, R. Bai, Membrane fouling and cleaning in microfiltration of activated sludge wastewater, J. Memb. Sci. 216 (2003) 279–290, doi:10.1016/S0376-7388(03)00083-8.
[3] L. Song, Flux decline in crossflow microfiltration and ultrafiltration: mechanisms and modeling of membrane fouling, J. Memb. Sci. 139 (1998) 183–200, doi:10.1016/S0376-7388(97)00263-9.
[4] P. Rajala, M. Bomberg, E. Huttunen-Saarivirta, O. Priha, M. Tausa, L. Carpén, Influence of chlorination and choice of materials on fouling in cooling water system under brackish seawater conditions, Materials 9 (2016), doi:10.3390/ma9060475.
[5] K.M. Bataineh, Multi-effect desalination plant combined with thermal compressor driven by steam generated by solar energy, DES 385 (2016) 39–52, doi:10.1016/j.desal.2016.02.011.
[6] M. Lejars, A. Margaillan, C. Bressy, Fouling release coatings: a nontoxic alternative to biocidal antifouling coatings, Chem. Rev. 112 (2012) 4347–4390, doi:10.1021/cr200350v.
[7] R.F. Brady, Properties which influence marine fouling resistance in polymers containing silicon and fluorine, Prog. Org. Coat. 35 (1999) 31–35, doi:10.1016/S0300-9440(99)00005-3.
[8] A.G. Nurioglu, A.C.C. Esteves, G. De With, Non-toxic, non-biocide-release antifouling coatings based on molecular structure design for marine applications, J. Mater. Chem. B. 3 (2015) 6547–6570, doi:10.1039/c5tb00232j.
[9] F. Wang, V.V. Tarabara, Pore blocking mechanisms during early stages of membrane fouling by colloids, J. Colloid Interface Sci. 328 (2008) 464–469, doi:10.1016/j.jcis.2008.09.028.
[10] T.H. Bae, T.M. Tak, Effect of TiO2 nanoparticles on fouling mitigation of ultrafiltration membranes for activated sludge filtration, J. Memb. Sci. 249 (2005) 1–8, doi:10.1016/j.memsci.2004.09.008.
[11] Z. Wang, D. Hou, S. Lin, Composite membrane with underwater-oleophobic surface for anti-oil-fouling membrane distillation, Environ. Sci. Technol. 50 (2016) 3866–3874, doi:10.1021/acs.est.5b05976.
[12] F. Meng, S.R. Chae, A. Drews, M. Kraume, H.S. Shin, F. Yang, Recent advances in membrane bioreactors (MBRs): membrane fouling and membrane material, Water Res 43 (2009) 1489–1512, doi:10.1016/j.watres.2008.12.044.
[13] K. Chon, S. Sarp, S. Lee, J.H. Lee, J.A. Lopez-Ramirez, J. Cho, Evaluation of a membrane bioreactor and nanofiltration for municipal wastewater reclamation: trace contaminant control and fouling mitigation, Desalination 272 (2011) 128–134, doi:10.1016/j.desal.2011.01.002.
[14] Z. Wang, Z. Wu, X. Yin, L. Tian, Membrane fouling in a submerged membrane bioreactor (MBR) under sub-critical flux operation: membrane foulant and gel layer characterization, J. Memb. Sci. 325 (2008) 238–244, doi:10.1016/j.memsci.2008.07.035.
[15] W. Wang, X. Du, H. Vahabi, S. Zhao, Y. Yin, A.K. Kota, T. Tong, Trade-off in membrane distillation with monolithic omniphobic membranes, Nat. Commun. 10 (2019) 1–9, doi:10.1038/s41467-019-11209-6.
[16] J.E. Gittens, T.J. Smith, R. Suleiman, R. Akid, Current and emerging environmentally-friendly systems for fouling control in the marine environment, Biotechnol. Adv. 31 (2013) 1738–1753, doi:10.1016/j.biotechadv.2013.09.002.
[17] T. Horseman, Y. Yin, K.S. Christie, Z. Wang, T. Tong, S. Lin, Wetting, scaling, and fouling in membrane distillation: state-of-the-art insights on fundamental mechanisms and mitigation strategies, ACS ES&T Eng. 1 (2021) 117–140, doi:10.1021/acsestengg.0c00025.
[18] P. Rajala, E. Sohlberg, O. Priha, I. Tsitko, H. Väisänen, M. Tausa, L. Carpén, Biofouling on coated carbon steel in cooling water cycles using brackish seawater, J. Mar. Sci. Eng. (2016) 4, doi:10.3390/jmse4040074.
[19] S. Lee, J. Cho, M. Elimelech, Combined influence of natural organic matter (NOM) and colloidal particles on nanofiltration membrane fouling, J. Memb. Sci. 262 (2005) 27–41, doi:10.1016/j.memsci.2005.03.043.
[20] S. Hong, M. Elimelech, Chemical and physical aspects of natural organic matter (NOM) fouling of nanofiltration membranes, J. Memb. Sci. 132 (1997) 159–181, doi:10.1016/S0376-7388(97)00060-4.
[21] T. Mohammadi, M. Kazemimoghadam, M. Saadabadi, Modeling of membrane fouling and flux decline in reverse osmosis during separation of oil in water emulsions, Desalination 157 (2003) 369–375, doi:10.1016/S0011-9164(03)00419-3.
[22] I.M.A. Elsherbiny, A.S.G. Khalil, M. Ulbricht, Influence of surface micro-patterning and hydrogel coating on colloidal silica fouling of polyamide thin-film composite membranes, Membranes 9 (2019), doi:10.3390/membranes9060067.
[23] D. Ferrando, D. Toubiana, N.S. Kandiyote, T.H. Nguyen, A. Nejidat, M. Herzberg, Ambivalent role of calcium in the viscoelastic properties of extracellular polymeric substances and the consequent fouling of reverse osmosis membranes, Desalination 429 (2018) 12–19, doi:10.1016/j.desal.2017.12.006.
[24] S. Shao, H. Liang, F. Qu, K. Li, H. Chang, H. Yu, G. Li, Combined influence by humic acid (HA) and powdered activated carbon (PAC) particles on ultrafiltration membrane fouling, J. Memb. Sci. 500 (2016) 99–105, doi:10.1016/j.memsci.2015.11.036.
[25] C. Combe, E. Molis, P. Lucas, R. Riley, M.M. Clark, The effect of CA membrane properties on adsorptive fouling by humic acid, J. Memb. Sci. 154 (1999) 73–87, doi:10.1016/S0376-7388(98)00268-3.
[26] T. Knoell, J. Safarik, T. Cormack, R. Riley, S.W. Lin, H. Ridgway, Biofouling potentials of microporous polysulfone membranes containing a sulfonated polyether-ethersulfone/polyethersulfone block copolymer: correlation of membrane surface properties with bacterial attachment, J. Memb. Sci. 157 (1999) 117–138, doi:10.1016/S0376-7388(98)00365-2.
[27] X. Zhu, M. Elimelech, Colloidal fouling of reverse osmosis membranes: measurements and fouling mechanisms, Environ. Sci. Technol. 31 (1997) 3654–3662, doi:10.1021/es970400v.
[28] Y. Li, S. Shi, H. Cao, Z. Zhao, C. Su, H. Wen, Improvement of the antifouling performance and stability of an anion exchange membrane by surface modification with graphene oxide (GO) and polydopamine (PDA), J. Memb. Sci. 566 (2018) 44–53, doi:10.1016/j.memsci.2018.08.054.
[29] G. Mustafa, K. Wyns, S. Janssens, A. Buekenhoudt, V. Meynen, Evaluation of the fouling resistance of methyl grafted ceramic membranes for inorganic foulants and co-effects of organic foulants, Sep. Purif. Technol. 193 (2018) 29–37, doi:10.1016/j.seppur.2017.11.015.
[30] R.R. Choudhury, J.M. Gohil, S. Mohanty, S.K. Nayak, Antifouling, fouling release and antimicrobial materials for surface modification of reverse osmosis and nanofiltration membranes, J. Mater. Chem. A 6 (2018) 313–333, doi:10.1039/c7ta08627j.
[31] C. Boo, S. Hong, M. Elimelech, Relating organic fouling in membrane distillation to intermolecular adhesion forces and interfacial surface energies, Environ. Sci. Technol. 52 (2018) 14198–14207, doi:10.1021/acs.est.8b05768.
[32] E.M. Vrijenhoek, S. Hong, M. Elimelech, Influence of membrane surface properties on initial rate of colloidal fouling of reverse osmosis and nanofiltration membranes, J. Memb. Sci. 188 (2001) 115–128, doi:10.1016/S0376-7388(01)00376-3.
[33] E.M.V Hoek, S. Bhattacharjee, M. Elimelech, Effect of membrane surface roughness on colloid-membrane DLVO interactions, Langmuir 19 (2003) 4836–4847, doi:10.1021/la027083c.
[34] Q. Li, Z. Xu, I. Pinnau, Fouling of reverse osmosis membranes by biopolymers in wastewater secondary effluent: role of membrane surface properties and initial permeate flux, J. Memb. Sci. 290 (2007) 173–181, doi:10.1016/j.memsci.2006.12.027.
[35] D. Rana, T. Matsuura, Surface modifications for antifouling membranes, Chem. Rev. 110 (2010) 2448–2471, doi:10.1021/cr800208y.
[36] L. Yan, Y.S. Li, C.B. Xiang, S. Xianda, Effect of nano-sized Al_2O_3-particle addition on PVDF ultrafiltration membrane performance, J. Memb. Sci. 276 (2006) 162–167, doi:10.1016/j.jsb.2006.03.024.
[37] F. Li, J. Meng, J. Ye, B. Yang, Q. Tian, C. Deng, Surface modification of PES ultrafiltration membrane by polydopamine coating and poly(ethylene glycol) grafting: morphology, stability, and anti-fouling, Desalination 344 (2014) 422–430, doi:10.1016/j.desal.2014.04.011.
[38] R. Zhang, Y. Li, Y. Su, X. Zhao, Y. Liu, X. Fan, T. Ma, Z. Jiang, Engineering amphiphilic nanofiltration membrane surfaces with a multi-defense mechanism for improved antifouling performances, J. Mater. Chem. A 4 (2016) 7892–7902, doi:10.1039/C6TA02885C.
[39] D. Hou, K.S.S. Christie, K. Wang, M. Tang, D. Wang, J. Wang, Biomimetic superhydrophobic membrane for membrane distillation with robust wetting and fouling resistance, J. Memb. Sci. 599 (2020) 117708, doi:10.1016/j.memsci.2019.117708.
[40] X. Lu, Y. Peng, L. Ge, R. Lin, Z. Zhu, S. Liu, Amphiphobic PVDF composite membranes for anti-fouling direct contact membrane distillation, J. Memb. Sci. 505 (2016) 61–69, doi:10.1016/j.memsci.2015.12.042.
[41] H. Shan, J. Liu, X. Li, Y. Li, F.H. Tezel, B. Li, S. Wang, Nanocoated amphiphobic membrane for flux enhancement and comprehensive anti-fouling performance in direct contact membrane distillation, J. Memb. Sci. 567 (2018) 166–180, doi:10.1016/j.memsci.2018.09.038.
[42] W. Zhang, Y. Li, J. Liu, B. Li, S. Wang, Fabrication of hierarchical poly (vinylidene fluoride) micro/nano-composite membrane with anti-fouling property for membrane distillation, J. Memb. Sci. 535 (2017) 258–267, doi:10.1016/j.memsci.2017.04.051.
[43] Z. Wang, D. Hou, S. Lin, Composite membrane with underwater-oleophobic surface for anti-oil-fouling membrane distillation, Environ. Sci. Technol. (2016) acs.est.5b05976, doi:10.1021/acs.est.5b05976.
[44] G. Zuo, R. Wang, Novel membrane surface modification to enhance anti-oil fouling property for membrane distillation application, J. Memb. Sci. 447 (2013) 26–35, doi:10.1016/j.memsci.2013.06.053.
[45] K. Wang, D. Hou, J. Wang, Z. Wang, B. Tian, P. Liang, Hydrophilic surface coating on hydrophobic PTFE membrane for robust anti-oil-fouling membrane distillation, Appl. Surf. Sci. 450 (2018) 57–65, doi:10.1016/j.apsusc.2018.04.180.

[46] D. Hou, Z. Wang, K. Wang, J. Wang, S. Lin, Composite membrane with electrospun multiscale-textured surface for robust oil-fouling resistance in membrane distillation, J. Memb. Sci. 546 (2018) 179–187, doi:10.1016/j.memsci.2017.10.017.
[47] S. Meng, Y. Ye, J. Mansouri, V. Chen, Fouling and crystallization behavior of superhydrophobic nano-composite PVDF membranes in direct contact membrane distillation, J. Memb. Sci. 463 (2014) 102–112, doi:10.1016/j.memsci.2014.03.027.
[48] M. Khayet, A. Velázquez, J.I. Mengual, Direct contact membrane distillation of humic acid solutions, J. Memb. Sci. 240 (2004) 123–128, doi:10.1016/j.memsci.2004.04.018.
[49] A. Bogler, S. Lin, E. Bar-Zeev, Biofouling of membrane distillation, forward osmosis and pressure retarded osmosis: principles, impacts and future directions, J. Memb. Sci. 542 (2017) 378–398, doi:10.1016/j.memsci.2017.08.001.
[50] E. Bar-Zeev, U. Passow, S. Romero-Vargas Castrillón, M. Elimelech, Transparent exopolymer particles: from aquatic environments and engineered systems to membrane biofouling, Environ. Sci. Technol. 49 (2015) 691–707, doi:10.1021/es5041738.
[51] S.H. Flint, P.J. Bremer, J. Brooks, Biofilms in dairy manufacturing plant - description, current concerns and methods of control, Biofouling J. Bioadhesion Biofilm Res. 11 (1) (1997) 81–97.
[52] R.L. Fletcher, M.E. Callow, The settlement, attachment and establishment of marine algal spores, Br. Phycol. J. 27 (1992) 303–329, doi:10.1080/00071619200650281.
[53] D. Howell, B. Behrends, A review of surface roughness in antifouling coatings illustrating the importance of cutoff length, Biofouling 22 (2006) 401–410, doi:10.1080/08927010601035738.
[54] S. García, A. Trueba, L.M. Vega, E. Madariaga, Impact of the surface roughness of AISI 316L stainless steel on biofilm adhesion in a seawater-cooled tubular heat exchanger-condenser, Biofouling 32 (2016) 1185–1193, doi:10.1080/08927014.2016.1241875.
[55] A.J. Scardino, E. Harvey, R. De Nys, Testing attachment point theory: diatom attachment on microtextured polyimide biomimics, Biofouling 22 (2006) 55–60, doi:10.1080/08927010500506094.
[56] A.J. Scardino, J. Guenther, R. de Nys, Attachment point theory revisited: the fouling response to a microtextured matrix, Biofouling 24 (2008) 45–53, doi:10.1080/08927010701784391.
[57] M.L. Carman, T.G. Estes, A.W. Feinberg, J.F. Schumacher, W. Wilkerson, L.H. Wilson, M.E. Callow, J.A. Callow, A.B. Brennan, Engineered antifouling microtopographies - correlating wettability with cell attachment, Biofouling 22 (2006) 11–21, doi:10.1080/08927010500484854.
[58] L. Hoipkemeier-Wilson, J.F. Schumacher, M.L. Carman, A.L. Gibson, A.W. Feinberg, M.E. Callow, J.A. Finlay, J.A. Callow, A.B. Brennan, Antifouling potential of lubricious, micro-engineered, PDMS elastomers against zoospores of the green fouling alga Ulva (Enteromorpha), Biofouling 20 (2004) 53–63, doi:10.1080/08927010410001662689.
[59] D.Z. Liu, S. Jindal, J. Amamcharla, S. Anand, L. Metzger, Short communication: evaluation of a sol-gel–based stainless steel surface modification to reduce fouling and biofilm formation during pasteurization of milk, J. Dairy Sci. 100 (2017) 2577–2581, doi:10.3168/jds.2016-12141.
[60] S. Jindal, S. Anand, K. Huang, J. Goddard, L. Metzger, J. Amamcharla, Evaluation of modified stainless steel surfaces targeted to reduce biofilm formation by common milk sporeformers, J. Dairy Sci. 99 (2016) 9502–9513, doi:10.3168/jds.2016-11395.
[61] W. Stöber, A. Fink, Controlled growth of monodisperse silica spheres in the micron size range, J. Colloid Interface Sci. 26 (1968) 62–69, doi:10.1589/jpts.29.112.
[62] A. Papra, N. Gadegaard, N.B. Larsen, Characterization of ultrathin poly(ethylene glycol) monolayers on silicon substrates, Langmuir 17 (2001) 1457–1460, doi:10.1021/la000609d.
[63] C. Boo, J. Lee, M. Elimelech, Omniphobic Polyvinylidene fluoride (PVDF) membrane for desalination of shale gas produced water by membrane distillation, Environ. Sci. Technol. 50 (2016) 12275–12282, doi:10.1021/acs.est.6b03882.
[64] Q. Li, M. Elimelech, Organic fouling and chemical cleaning of nanofiltration membranes: measurements and mechanisms, Environ. Sci. Technol. 38 (2004) 4683–4693, doi:10.1021/es0354162.
[65] S. Assemi, J. Nalaskowski, W.P. Johnson, Direct force measurements between carboxylate-modified latex microspheres and glass using atomic force microscopy, Colloids Surf. A Physicochem. Eng. Asp. 286 (2006) 70–77, doi:10.1016/j.colsurfa.2006.03.024.
[66] A. Filby, M. Plaschke, H. Geckeis, AFM force spectroscopy study of carboxylated latex colloids interacting with mineral surfaces, Colloids Surf. A Physicochem. Eng. Asp. 414 (2012) 400–414, doi:10.1016/j.colsurfa.2012.08.040.
[67] A.V. Nguyen, J. Nalaskowski, J.D. Miller, H.J. Butt, Attraction between hydrophobic surfaces studied by atomic force microscopy, Int. J. Miner. Process. 72 (2003) 215–225, doi:10.1016/S0301-7516(03)00100-5.
[68] A. Seidel, M. Elimelech, Coupling between chemical and physical interactions in natural organic matter (NOM) fouling of nanofiltration membranes: implications for fouling control, J. Memb. Sci. 203 (2002) 245–255, doi:10.1016/S0376-7388(02)00013-3.
[69] A.R. Costa, M.N. de Pinho, M. Elimelech, Mechanisms of colloidal natural organic matter fouling in ultrafiltration, J. Memb. Sci. 281 (2006) 716–725, doi:10.1016/j.memsci.2006.04.044.
[70] S. Lee, M. Elimelech, Relating organic fouling of reverse osmosis membranes to intermolecular adhesion forces, Environ. Sci. Technol. 40 (2006) 980–987, doi:10.1021/es051825h.
[71] R.J. Hunter, Foundations of Colloid Science, 2nd ed., Oxford University Press, 2001.
[72] J. Israelachvili, Intermolecular and Surface Forces, 3rd ed., Elsevier Inc, Waltham, MA, 2011.
[73] M. Elimelech, J. Gregory, X. Jia, Particle Deposition and Aggregation: Measurement, Modeling and Simulation, Butterworth-Heinemann, 2013.
[74] J. Drelich, E. Chibowski, Superhydrophilic and superwetting surfaces: definition and mechanisms of control, Langmuir 26 (2010) 18621–18623, doi:10.1021/la1039893.
[75] R.N. Wenzel, Surface roughness and contact angle, J. Phys. Colloid Chem. 53 (1949) 1466–1467, doi:10.1021/j150474a015.
[76] A. Marmur, Wetting on hydrophobic rough surfaces: to be heterogeneous or not to be? Langmuir 19 (2003) 8343–8348, doi:10.1021/la0344682.
[77] A.B.D. Cassie, Contact angles, Discuss. Faraday Soc. 3 (1948) 11, doi:10.1039/df9480300011.
[78] C. Su, T. Horseman, H. Cao, K. Christie, Y. Li, S. Lin, Robust superhydrophobic membrane for membrane distillation with excellent scaling resistance, Environ. Sci. Technol. 53 (2019) 11801–11809, doi:10.1021/acs.est.9b04362.
[79] T. Horseman, C. Su, K.S.S. Christie, S. Lin, Highly effective scaling mitigation in membrane distillation using a superhydrophobic membrane with gas purging, Environ. Sci. Technol. Lett. 6 (2019) 423–429, doi:10.1021/acs.estlett.9b00354.
[80] vasiliki Karanikola, C. Boo, J. Rolf, M. Elimelech, Engineered slippery surface to mitigate gypsum scaling in membrane distillation for treatment of hypersaline industrial wastewaters, Environ. Sci. Technol. 52 (2018) 14362–14370, doi:10.1021/acs.est.8b04836.
[81] L. Xu, R.G. Karunakaran, J. Guo, S. Yang, Transparent, Superhydrophobic Surfaces from One-Step Spin Coating of Hydrophobic Nanoparticles, ACS applied materials & interfaces, 2012.
[82] M. Hikita, K. Tanaka, T. Nakamura, T. Kajiyama, A. Takahara, Super-liquid-repellent surfaces prepared by colloidal silica nanoparticles covered with fluoroalkyl groups, Langmuir 21 (2005) 7299–7302, doi:10.1021/la050901r.
[83] J. Li, S. Guo, Z. Xu, J. Li, Z. Pan, Z. Du, F. Cheng, Preparation of omniphobic PVDF membranes with silica nanoparticles for treating coking wastewater using direct contact membrane distillation: electrostatic adsorption vs. chemical bonding, J. Memb. Sci. 574 (2019) 349–357, doi:10.1016/j.memsci.2018.12.079.
[84] Y. Liao, C.H. Loh, R. Wang, A.G. Fane, Electrospun superhydrophobic membranes with unique structures for membrane distillation, ACS Appl. Mater. Interfaces 6 (2014) 16035–16048, doi:10.1021/am503968n.
[85] R.M. Pashley, Hydration forces between mica surfaces in aqueous electrolyte solutions, J. Colloid Interface Sci. 80 (1981) 153–162, doi:10.1016/0021-9797(81)90171-5.
[86] S. Chen, L. Li, C. Zhao, J. Zheng, Surface hydration: principles and applications toward low-fouling/nonfouling biomaterials, Polymer 51 (2010) 5283–5293, doi:10.1016/j.polymer.2010.08.022.
[87] J. Israelachvili, R. Pashley, The hydrophobic interaction is long range, decaying exponentially with distance, Nature 300 (1982) 341–342, doi:10.1038/300341a0.
[88] Y. Tsao, D. Evans, H. Wennerstrom, Long-range attractive force between hydrophobic surfaces observed by atomic force microscopy, Science 262 (1993) 547–550, doi:10.1126/science.8211182.
[89] E.E. Meyer, K.J. Rosenberg, J. Israelachvili, Recent progress in understanding hydrophobic interactions, Proc. Natl. Acad. Sci. U. S. A. 103 (2006) 15739–15746, doi:10.1073/pnas.0606422103.
[90] D.M. Warsinger, J. Swaminathan, E. Guillen-Burrieza, H.A Arafat, J.H. Lienhard, V, Scaling and fouling in membrane distillation for desalination applications: a review, Desalination 356 (2014) 294–313, doi:10.1016/j.desal.2014.06.031.
[91] H.J. Butt, Measuring electrostatic, van der Waals, and hydration forces in electrolyte solutions with an atomic force microscope, Biophys. J. 60 (1991) 1438–1444, doi:10.1016/S0006-3495(91)82180-4.
[92] W.A. Ducker, T.J. Senden, R.M. Pashley, Measurement of forces in liquids using a force microscope, Langmuir 8 (1992) 1831–1836, doi:10.1021/la00043a024.
[93] S. Veeramasuneni, M.R. Yalamanchili, J.D. Miller, Measurement of interaction forces between silica and α-alumina by atomic force microscopy, J. Colloid Interface Sci. 184 (1996) 594–600, doi:10.1006/jcis.1996.0656.
[94] A. Faghihnejad, H. Zeng, Interaction mechanism between hydrophobic and hydrophilic surfaces: using polystyrene and mica as a model system, Langmuir 29 (2013) 12443–12451, doi:10.1021/la402244h.
[95] D.J. Babu, M. Mail, W. Barthlott, J.J. Schneider, Superhydrophobic vertically aligned carbon nanotubes for biomimetic air retention under water (Salvinia Effect), Adv. Mater. Interfaces 4 (2017) 1–6, doi:10.1002/admi.201700273.
[96] J.H. Lee, J.C. Meredith, Non-DLVO silica interaction forces in NMP-water mixtures. II. An asymmetric system, Langmuir 27 (2011) 10000–10006, doi:10.1021/la202176u.
[97] A.P. Serro, R. Colaço, B. Saramago, Adhesion forces in liquid media: effect of surface topography and wettability, J. Colloid Interface Sci. 325 (2008) 573–579, doi:10.1016/j.jcis.2008.05.032.
[98] H. Seo, M. Yoo, S. Jeon, Influence of nanobubbles on the adsorption of nanoparticles, Langmuir 23 (2007) 1623–1625, doi:10.1021/la062763r.
[99] A. Carambassis, L.C. Jonker, P. Attard, M.W. Rutland, Forces measured between hydrophobic surfaces due to a submicroscopic bridging bubble, Phys. Rev. Lett. 80 (1998) 5357–5360, doi:10.1103/PhysRevLett.80.5357.
[100] A.M. Smith, M. Borkovec, G. Trefalt, Forces between solid surfaces in aqueous electrolyte solutions, Adv. Colloid Interface Sci. 275 (2020) 102078, doi:10.1016/j.cis.2019.102078.
[101] N. Daems, S. Milis, R. Verbeke, A. Szymczyk, P.P. Pescarmona, I.F.J. Vankelecom, High-performance membranes with full pH-stability, RSC Adv. 8 (2018) 8813–8827, doi:10.1039/c7ra13663c.
[102] G. Werner, H. Körber, R. Zimmermann, S. Dukhin, H.J. Jacobasch, Extended electrokinetic characterization of flat solid surfaces, J. Colloid Interface Sci. 208 (1998) 329–346, doi:10.1006/jcis.1998.5787.

[103] T. Xu, R. Fu, L. Yan, A new insight into the adsorption of bovine serum albumin onto porous polyethylene membrane by zeta potential measurements, FTIR analyses, and AFM observations, J. Colloid Interface Sci. 262 (2003) 342–350, doi:10.1016/S0021-9797(03)00208-X.
[104] H. Al-Shehri, T.S. Horozov, V.N. Paunov, Adsorption of carboxylic modified latex particles at liquid interfaces studied by the gel trapping technique, Soft Matter 10 (2014) 6433–6441, doi:10.1039/c4sm01030b.
[105] K.E. Cooksey, B. Wigglesworth-Cooksey, Adhesion of bacteria and diatoms to surfaces in the sea: a review, Aquat. Microb. Ecol. 9 (1995) 87–96, doi:10.3354/ame009087.
[106] M. Fletcher, G.I. Loeb, Influence of Substratum Characteristics on the Attachment of a Marine Pseudomonad to Solid Surfaces, Appl. Environ. Microbiol. 37 (1979) 67–72, doi:10.1128/aem.37.1.67-72.1979.
[107] S. Holberg, R. Losada, F.H. Blaikie, H.H.W.B. Hansen, S. Soreau, R.C.A. Onderwater, Hydrophilic silicone coatings as fouling release: simple synthesis, comparison to commercial, marine coatings and application on fresh water-cooled heat exchangers, Mater. Today Commun. 22 (2020) 100750, doi:10.1016/j.mtcomm.2019.100750.
[108] A.M.S. El Din, M.E. El-Dahshan, A.M.T. El Din, Bio-film formation on stainless steels part 2. The role of seasonal changes, seawater composition and surface roughness, Desalination 154 (2003) 267–276, doi:10.1016/S0011-9164(03)80042-5.
[109] M.I. Baoxia, M. Elimelech, Gypsum scaling and cleaning in forward osmosis: measurements and mechanisms, Environ. Sci. Technol. 44 (2010) 2022–2028, doi:10.1021/es903623r.
[110] B. Mi, M. Elimelech, Organic fouling of forward osmosis membranes: fouling reversibility and cleaning without chemical reagents, J. Memb. Sci. 348 (2010) 337–345, doi:10.1016/j.memsci.2009.11.021.
[111] C. Shi, D.Y.C. Chan, Q. Liu, H. Zeng, Probing the Hydrophobic Interaction Between Air Bubbles and Partially Hydrophobic Surfaces Using Atomic Force Microscopy, The Journal of Physical Chemistry C, 2014.